Supplementary Information for:

Sorption of metal ions onto PET-derived microplastic fibres

H. Frost[a,b], T. Bond[c,d], T. Sizmur[e] and M. Felipe-Sotelo[a]

a. School of Chemistry and Chemical Engineering, University of Surrey, Guildford, Surrey GU2 7XH, UK.

b. School of Civil Engineering and Surveying, University of Portsmouth, Portland Building, Portland Street, Portsmouth PO1 3AH, UK.

c. School of Sustainability, Civil and Environmental Engineering, University of Surrey, Guildford, GU2 7XH, UK

d. Water Research Centre, Frankland Rd, Swindon SN5 8YF, UK.

e. Department of Geography and Environmental Science, University of Reading, Reading, RG6 6DW, UK

Methods

Fibre characterisation

SEM Imaging

The morphology and surface topography of the PET fibres were observed using a scanning electron microscope (SEM) (Apreo SEM, ThermoFisher Scientific). The PET fabric and cryo-milled fibres were visually compared to identify the effect of cryo-milling on the surface morphology of the fibres. Samples were mounted on 12.7 mm aluminium stubs using double-sided carbon tape. Samples were then coated with a 6 nm layer of gold (Q150V ES Plus, Quorum). Prepared samples were observed using the SEM in secondary electron mode using the EDT and T1 detectors and the Optiplan user case. Samples were viewed with accelerating voltages of 1 – 15 kV, emission currents of 0.1 – 1.6 nA, and working distances of 3 – 10 mm. Images were taken at magnifications of 120 – 20,000×. Images with a resolution of 3072 by 2048 pixels were captured with a dwell time of 1 µs, and line integration was set to 8.

Raman spectroscopy

The functional groups of the PET fabric and fibres were characterised using Raman spectroscopy. Spectra were obtained for the PET fabric before and after rinsing in water, and for the cryo-milled fibres, using a Raman microscope (DXR3, ThermoScientific; U-TV0.5XC-3 microscope, Olympus) and a 50× objective lens. The Raman microscope was first calibrated, and the laser aligned using the calibration block. For spectra acquisition, the DXR 532 nm laser was used, with a laser power of 7 mW, and a 50 µm slit aperture. Each sample was subject to 30 seconds of photobleaching before spectra were obtained to reduce fluorescence. A short exposure time of 0.5 seconds was used to prevent overflow of the CCD (Charged Coupled Device) detector, and 24 exposures were combined for each spectrum to reduce noise. For comparison, spectra were normalised with respect to the highest intensity peak, which, for all spectra was the peak at approximately 1614 cm^{-1} corresponding to the C-C bonds of the aromatic ring.[1,2]. The library search feature of Spectragryph was used to identify samples by searching spectral databases for similar Raman spectra. The SLoPP (Spectral Libraries of Plastic Particles), SLoPP-E (Spectral Libraries of Plastic Particles Aged in the Environment), and RDWP (Raman Database of Weathered Microplastics) databases were used for identification.

Fibre dimensions

Fibre length and width data were obtained using optical microscopy. In a scintillation vial, a small amount of the PET fibres was suspended in hexane (≥ 95%; Sigma-Aldrich), and sonicated for 5 minutes. A dropper pipette was then used to apply a drop of the PET fibre suspension onto a clean microscope slide, which was examined using an Olympus DSX500 optical microscope equipped with a ×10 objective lens. After a few seconds to allow for hexane evaporation, four adjacent sections of each slide were imaged. Fibre lengths and widths were measured in ImageJ. Fibre lengths and widths were measured using a method adapted from Hernandez et al..[3] The scale for the images was set using embedded scale bars. The segmented straight-line tool was used to measure fibre length end-to-end. The straight-line tool was used to measure fibre widths, and an average of three equidistant measurements along each fibre was calculated. Average length and width data were collected using fibres from three separate milling cycles, and results were analysed using a one-way ANOVA to check for repeatability. Normal distributions of average fibre lengths and widths were produced.

Specific surface area

The specific surface area of the PET fibres was estimated using the fibre size measurements obtained using optical microscopy. Firstly, the surface area of each individual fibre was estimated using the following equation for the surface area of a cylinder, where A is the surface area (μm^2), r is the radius (µm) equal to half the average fibre width, and h is the fibre length (µm) (Equation SI-1).

Equation SI-1 $$A = 2\pi rh + 2\pi r^2$$

The volume of each individual fibre was then estimated using the following equation for the volume of a cylinder, where V is the volume (μm^3), r is the radius (µm) equal to half the average fibre width, and h is the fibre length (µm) (Equation SI-2).

Equation SI-2 $$V = \pi r^2 h$$

The mass of each fibre (M) was estimated by multiplying the volume of each fibre (converted to cm^3) by the average density (ρ) of PET, according to Henandez et al.[3] (1.365 g cm^3)[4] (Equation SI-3).

Equation SI-3 $$M = V \times \rho$$

Finally, the specific surface area (SSA) ($m^2\ g^{-1}$) (Equation SI-4) was calculated by dividing the average fibre surface area (A) (Equation SI-1) (converted to m^2), by the average fibre mass in grams (M) (Equation SI-3).

Equation SI-4 $$SSA = \frac{A}{M}$$

Zeta potential

The point of zero charge (pH_{PZC}) of PET fibres was derived from zeta potential measurements of fibre suspensions. Zeta potential was measured electrophoretically using a Zetamaster (Malvern Instruments, UK). Suspensions with a solid-to-liquid ratio of approximately 1:1000 were prepared in deionised water containing 0.001 M NaCl. Suspension pH was adjusted, as necessary, using drops of 0.1 M NaOH or 0.1 M HCl. Suspensions were sonicated and allowed to settle for 10 minutes before 10 mL was injected into the flow cell of the Zetamaster and the zeta potential was measured. Each sample was measured 10 times by the instrument, and

the flow cell was flushed three times with deionised water between samples. Measurements were obtained across a pH range of 1.5 – 11. Zeta potential was plotted across this pH range, and an approximate point of zero net charge was derived from the intersection point on the pH axis, as the approximate pH at which the zeta potential of the fibres in suspension was zero mV.

The pH_{PZC} was also calculated using the pH drift method.[5,6] 20 mL of 0.01 M NaCl solutions were prepared, and pH-adjusted over a range of 1-10, by adding drops of 0.1 M HCl and NaOH as necessary. The initial pH was measured using a pH probe, and 0.1 g of PET fibres was added to each solution. Controls which contained no PET fibres were also prepared to account for any pH change due to CO_2 dissolution/degasification. PET fibre suspensions and controls were placed on a rotary shaker for 24 hours at 20 rpm. Samples were then filtered (Whatman no. 1), and the final pH was measured. A graph was constructed with initial pH on the x axis, and pH change (initial pH – final pH) on the y axis. The point of intersection on the x axis (where pH change = 0), was taken as the estimated pH_{PZC}.[5,6]

Quantification of metal ions using inductively coupled plasma mass spectrometry (ICP-MS)

The instrument was first tuned using a tuning solution (1 µg L^{-1} cerium (Ce), cobalt (Co), lithium (Li), magnesium (Mg), titanium (Ti) and Yttrium (Y) in 2% HNO_3; Agilent Technologies). Pulse/analogue (P/A) factor adjustment was selected, to linearly calibrate analyte concentrations measured in both pulse mode (analyte ions are directed onto the detector in pulses), and analogue mode (analyte ions continually reach the detector). This compromises the high sensitivity of pulse mode, with the improved dynamic range of analogue mode. The samples were introduced using an autosampler, coupled to a peristaltic pump. The sample was nebulised, and the aerosol entered the 2 mm diameter orifice of the plasma torch through a double-pass spray chamber. An internal standard solution of 100 µg L^{-1} indium (^{115}In) was prepared in 1% HNO_3 by diluting an ICP-MS In standard solution (9941 mg L^{-1} indium in 1% HNO_3; DBH Laboratory Supplies, UK). The internal standard was introduced into the sample using a T-piece. The purpose of the internal standard is to allow for corrections of the analyte concentration due to changes in the instrument operating conditions or sample matrix effects which can enhance or supress the analyte signal throughout the operation of the instrument. Internal standard correction was performed by dividing the calibration blank-corrected analyte signal, in CPS (counts per second), by the internal standard signal, as shown in Equation SI-5.

Equation SI-5 $$Ratio = \frac{Analyte\ signal\ (CPS) - Calibration\ blank\ signal\ (CPS)}{Internal\ standard\ signal\ (CPS)}$$

Calibration was performed using a series of matrix-matched, multi-element calibration standards, containing 0, 1, 2.5, 5, 10, 25, 50, 100, 250 and 500 µg L^{-1} of each analyte. Calibration standard concentrations (x axis) were plotted against the ratio (y axis) for each calibration standard. The instrumental limit of detection (LOD) and limit of quantification (LOQ) (**Table SI-1**) were calculated for each element from a linear regression of their respective calibration curves, according to Equations SI-6 and SI-7, where; σ_y is the standard deviation of the intercept, and S is the slope. Analyte CPS were measured in sample and control (without PET fibres) filtrates. The linear slope and intercept were used to calculate the analyte concentrations in each sample, according to Equation SI-8. To eliminate potential polyatomic spectral interferences, all samples were run both with and without the He collision/reaction cell (CRC). Data selection was based on whether the analyte had expected polyatomic spectral interferences, the ISTD recovery and stability throughout the run, the linearity of the calibration curve, the relative standard deviation of the measurements, and the limits of detection. The autosampler probe was rinsed with 1% nitric acid between samples, and throughout the analysis, 1% nitric acid rinses were run as samples to check for carryover effects and contamination. Three nitric acid rinses were run before and after the calibration standards, and every 12 samples thereafter.

Equation SI-6 $$Limit\ of\ Detection\ (\mu g\ L^{-1}) = \frac{3 \times \sigma_y}{S}$$

Equation SI-7 $$Limit\ of\ Quantification\ (\mu g\ L^{-1}) = \frac{10 \times \sigma_y}{S}$$

Equation SI-8 $$Analyte\ concentration\ \mu g\ L^{-1} = \frac{Sample\ ratio - Intercept}{Slope}$$

Table SI-1: Instrumental limits of detection (LOD) and limits of quantification (LOQ) for the 12 metals analysed using ICP-MS during screening tests.

Analyte	LOD (µg L^{-1})	LOQ (µg L^{-1})
V	0.59	1.97
Cr	0.40	1.34
Co	0.36	1.19
Ni	0.98	3.27
Cu	1.70	5.67
Zn	1.59	5.29
As	0.81	2.70
Mo	0.56	1.86
Cd	0.55	1.83
Sb	0.48	1.61
Hg	3.40	11.32
Pb	0.49	1.62

Following the kinetic experiments, calibration was performed for Cd and Hg individually, with a series of matrix-matched calibration standards containing 0, 1, 2.5, 5, 10, 25, 50, 100, 250 and 500 µg L^{-1} of Cd or Hg. Hg standards were also spiked with 200 µg L^{-1} Au. Internal standard correction and analyte concentrations were calculated as described above. During Cd analysis, the autosampler probe was rinsed with 1% nitric acid between samples, and throughout the analysis, 1% nitric acid rinses were run as samples to check for carryover effects and contamination. Three nitric acid rinses were run before and after the calibration standards, and every 10-15 samples thereafter. During Hg analysis, the same rinse procedure was used but 200 µg L^{-1} Au in 1% HCl was used as the rinse solution.

Following isotherm trials, the ICP-MS was tuned as described above. Hg samples were diluted where necessary, to achieve an expected concentration of 100 µg L^{-1} or less. Calibration was performed with a series of matrix-matched calibration standards over a concentration range of 0 – 125 µg L^{-1} for Hg, and 0 – 250 µg L^{-1} for Cd. As before, Hg standards were also spiked with 200 µg L^{-1} Au. ^{115}In was used as an internal standard for Cd analysis, and ^{209}Bi (bismuth) was used as an internal standard for Hg analysis. Internal standard correction and analyte concentrations were calculated as described above. Cd and Hg concentrations were determined from the signals of the ^{111}Cd and ^{201}Hg isotopes respectively. For Cd analysis, 1% HNO_3 probe rinses were performed between samples. Two 1% HNO_3 rinses, a 100 µg L^{-1} quality control (QC) standard, and two more 1% HNO_3 rinses were run after the calibration standards, and every 10-15 samples thereafter. During Hg analysis, the same rinse procedure was used but 200 µg L^{-1} Au in 1% HCl was used as the rinse solution, and a 50 µg L^{-1} QC

standard was used. 10 replicate measurements of the calibration blank were performed for Cd and Hg. The instrument limit of detection (LOD) was calculated as 3× the standard deviation of these calibration blank measurements, and the limit of quantification (LOQ) was calculated as 10× the standard deviation (**Table SI-2**).

Table SI-2: Instrumental limits of detection (LOD), limits of quantification (LOQ), and average quality control (QC) standard recoveries for Cd and Hg analysis using ICP-MS during isotherm trials.

Analyte	pH	LOD (µg L^{-1})	LOQ (µg L^{-1})	Mean QC Standard Recovery (%)
Cd	6	0.051	0.171	109
	7	0.020	0.065	96.8
	8	0.073	0.242	100
Hg	6	0.024	0.081	105
	7	0.264	0.879	101
	8	0.058	0.195	99.6

Table SI-3: Monobasic and dibasic sodium phosphate masses used to prepare 0.1 mol L^{-1} phosphate buffers at pH 6, 7 and 8.

pH	Monobasic sodium phosphate ($NaH_2PO_4 \cdot H_2O$)		Dibasic sodium phosphate ($Na_2HPO_4 \cdot 2H_2O$)		Final volume with deionised water (L)
	Mass (g)	Concentration (mol L^{-1})	Mass (g)	Concentration (mol L^{-1})	
6	21.8576	0.0880	3.8446	0.0120	1.8
7	10.5066	0.0423	18.4860	0.0577	
8	1.6890	0.0068	29.8596	0.0932	

Kinetic models

Table SI-4: Kinetics and isotherm model equations, variables, derived parameters, and bounds used to fit kinetics models in Origin.

Kinetics Models		
	Pseudo-First Order Model	Pseudo-Second Order Model
Equation	qt = qe*(1-exp(-k1*t))	qt = qe^2*k2*t/(1+k2*qe*t)
Independent Variables	T	t
Dependent Variables	Qt	qt
Parameters	qe, k1	qe, k2
Bounds	0 < qe, 0 < k1	0 < qe, 0 < k2
Isotherm Models		
	Langmuir	Freundlich
Equation	$Cs = C_{SM}$ *b*Caq/(1+b*Caq)	Cs = Kf*Caq^(1/n)
Independent Variables	Caq	Caq
Dependent Variables	Cs	Cs
Parameters	C_{SM}, b	Kf, n
Bounds	0 < C_{SM}, 0 < b	0 < Kf, 0 < n

Results and Discussion

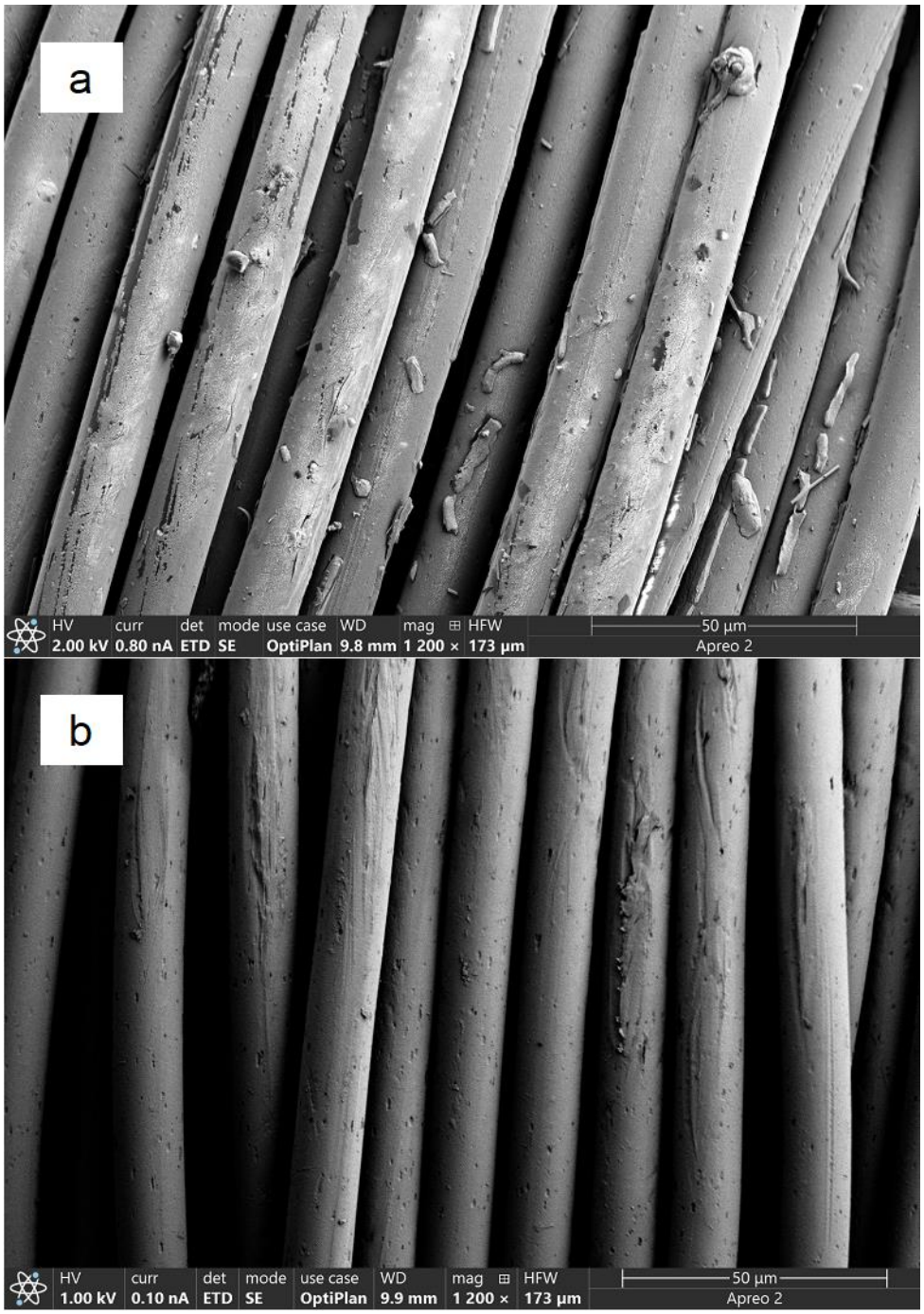

Figure SI-1: SEM images of the original PET fabric before cryo-milling (see section 4.2.1.). Images show the fabric before (a) and after (b) rinsing in water for 24 hours, at 1200× magnification.

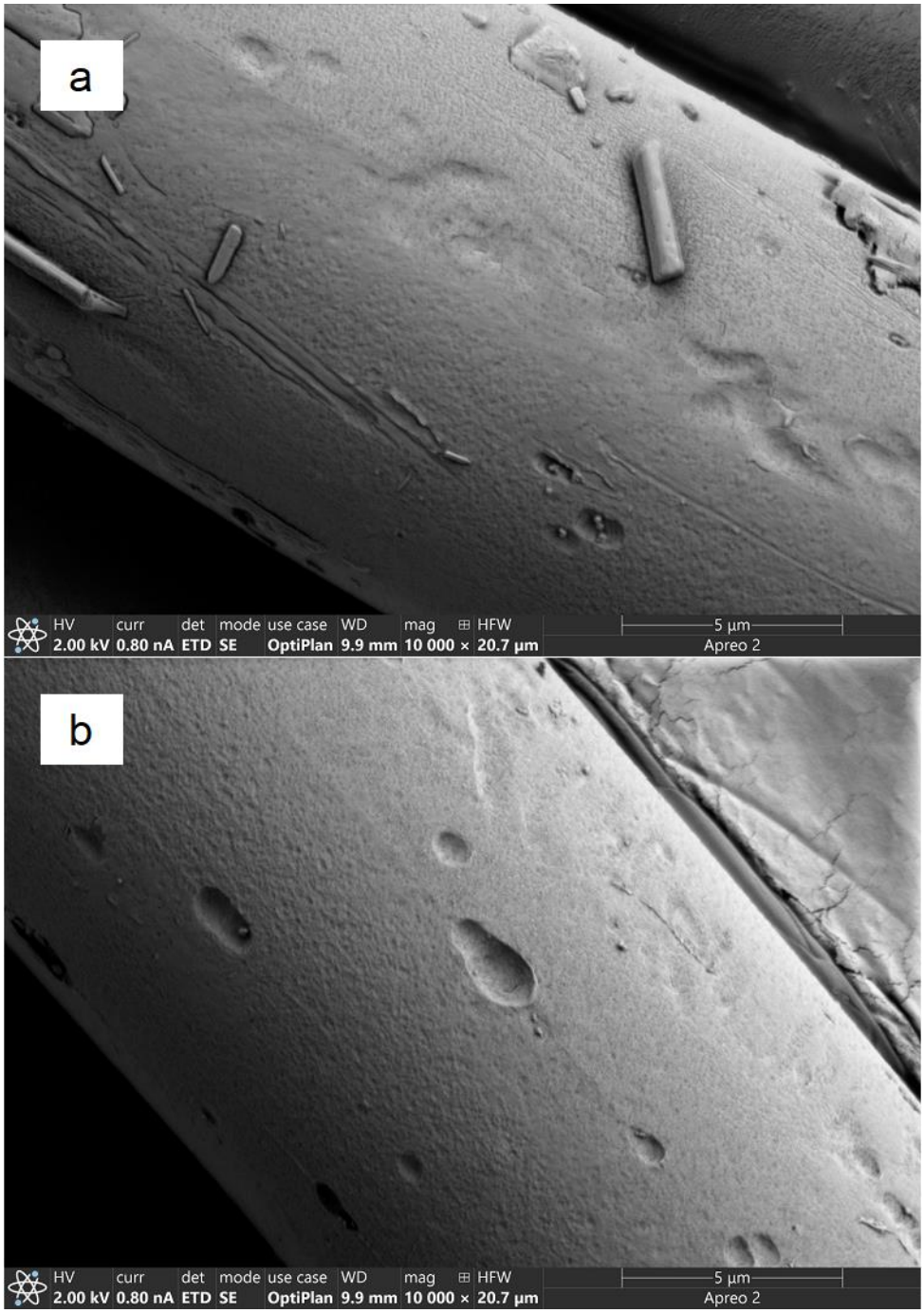

Figure SI-2: SEM images of the original PET fabric before cryo-milling (see section 4.2.1.). Images show individual fibres of the fabric before (a) and after (b) rinsing in water for 24 hours, at 10000× magnification.

Structure of polyethylene terephthalate (PET)

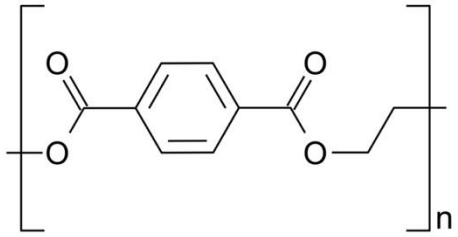

Peak Position (cm-1)	Assignment
279	Aromatic ring C-C
631	Aromatic ring C-C
858	Aromatic ring C-C
1094	Aromatic ring C-C C-C Ethylene Ester C-O (trans conformation)
1116	Aromatic ring C-H Ester C-O (gauche conformation)
1291	Aromatic ring C-C Ester C-O
1416	Aromatic ring C-C
1614	Aromatic ring C-C
1725	Carbonyl C=O
2964	Methylene C-H
3080	Aromatic ring C-H

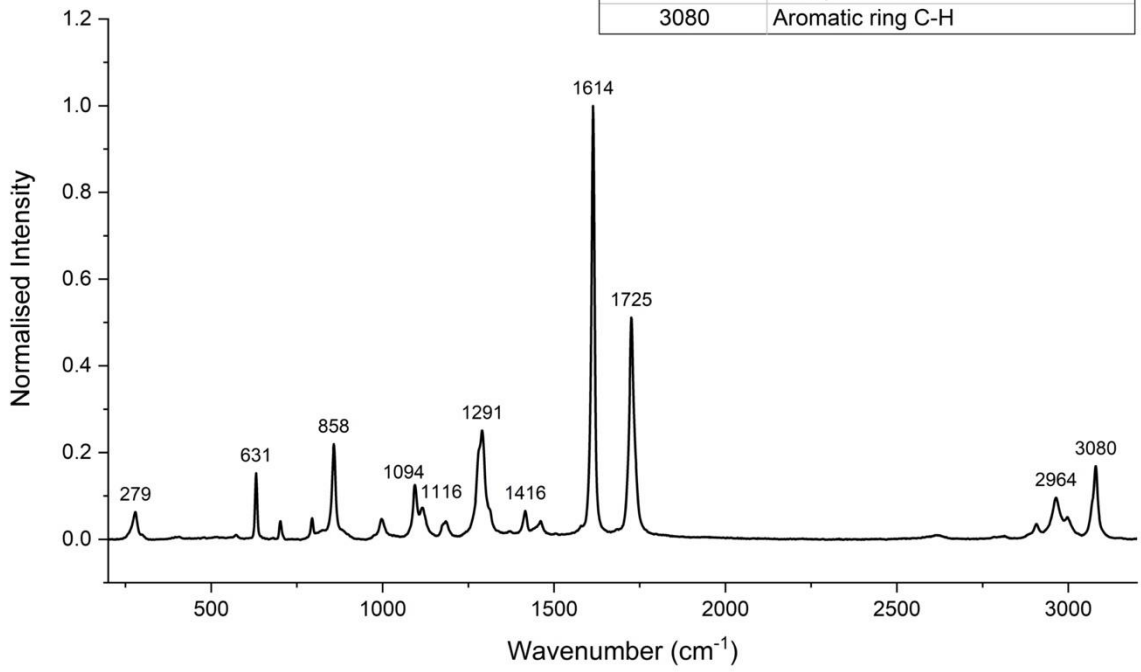

Figure SI-3.: Normalised Raman spectrum of the PET fabric, for a wavenumber range of 200 – 3200 cm^{-1}, with labelled peaks and assigned functional groups.

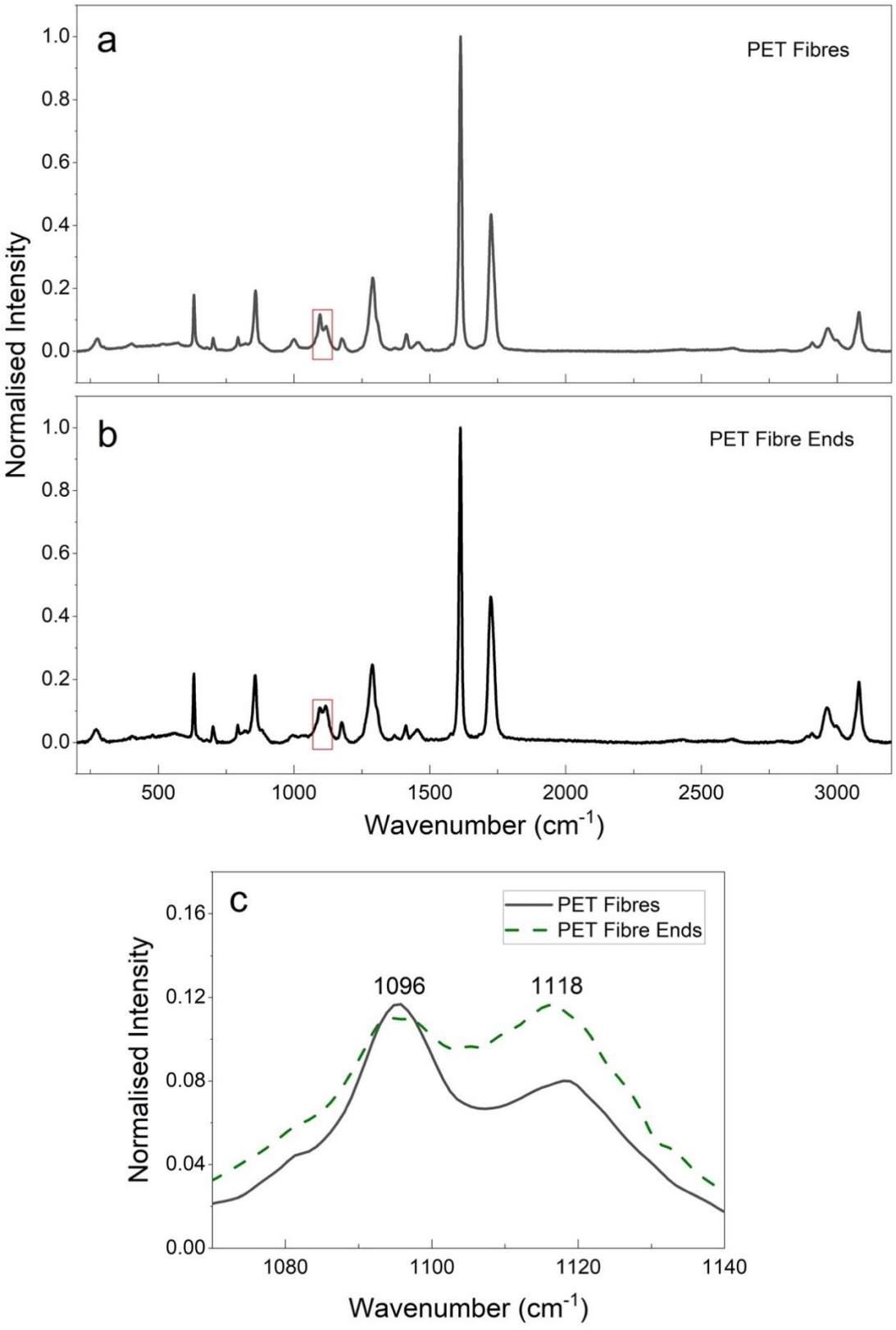

Figure SI-4: Normalised Raman spectra of the PET fibres (a) and fibre ends (b), over a wavenumber range of 200 – 3200 cm^{-1}. The double peaks at 1096 and 1118 cm^{-1}, highlighted in the red boxes, are compared (c).

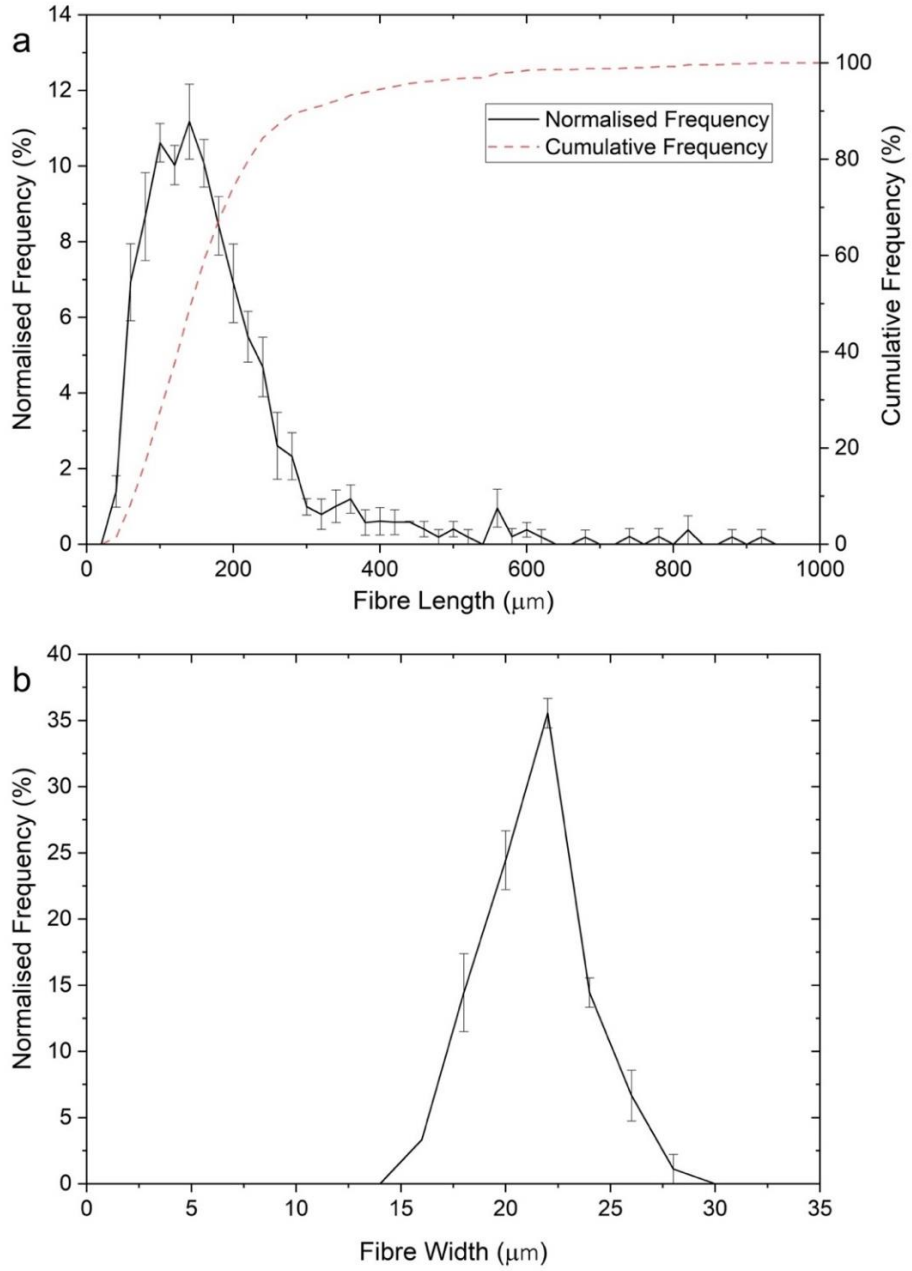

Figure SI-5: Normalised and cumulative fibre length (a) and width (b) distributions. Error bars show standard error (n = 3).

)

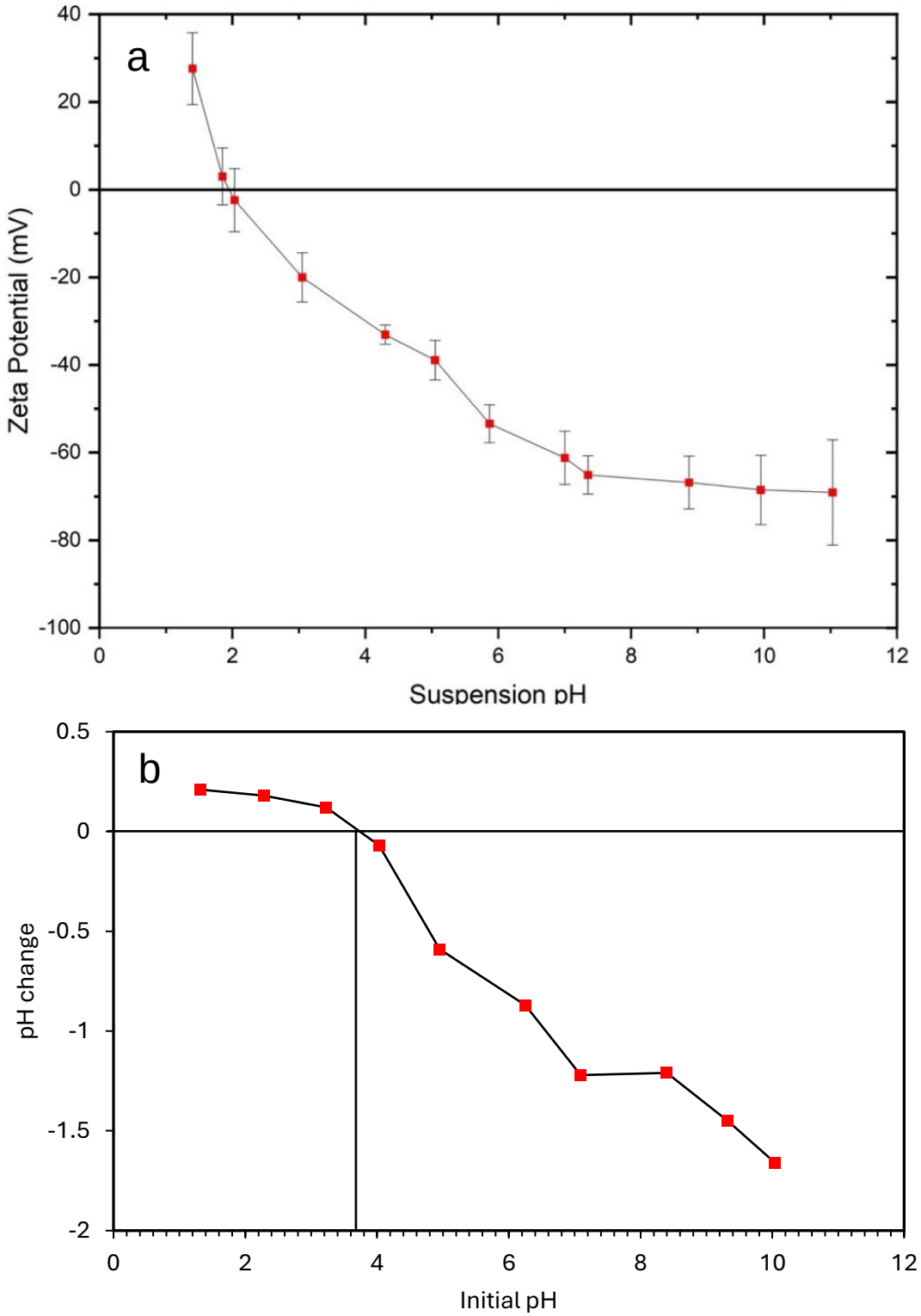

Figure SI-6: pH_{PZC} of PET fibres determined from two methods. Zeta potential measurements of PET fibre suspensions in 0.001 M NaCl, over a pH range of approximately 1.5 – 11 (a). Error bars show ± standard error (n = 10). pH drift curve with approximate pH_{PZC} determination (b).

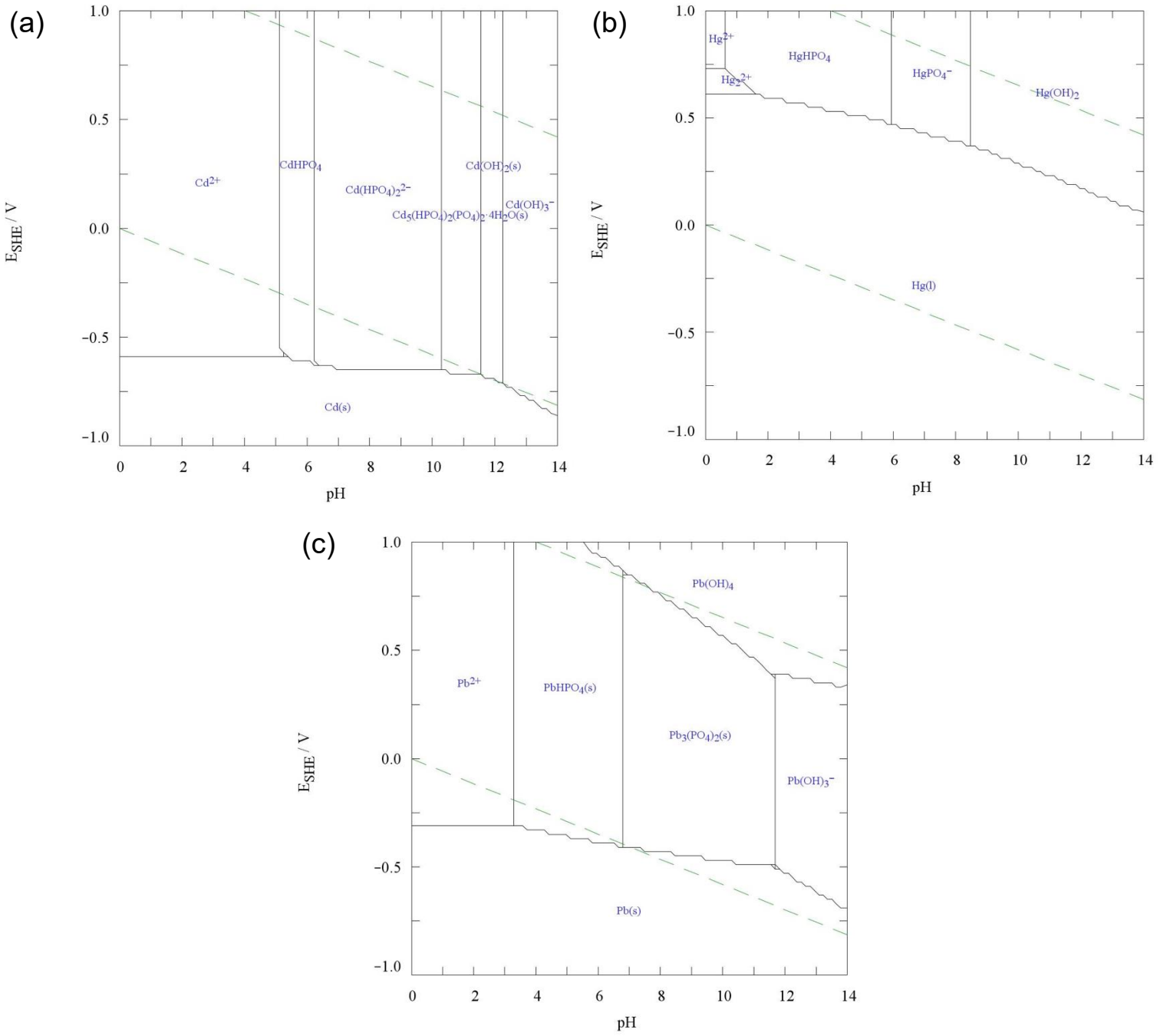

Figure SI-7: Calculated Pourbaix diagrams showing the predominant speciation of cadmium (a), mercury (b) and lead (c) as a function of pH and voltage potential with respect to a standard hydrogen electrode (E_{SHE}). Diagrams were created using MEDUSA. Temperature was 20 °C, ionic strength was fixed at 0.1 M (PO_4^{3-}), and metal concentrations for Cd, Pb and Hg were 1.78 µM (200 µg L^{-1}), 2.41 µM (500 µg L^{-1}), and 2.49 µM (500 µg L^{-1}), respectively.

References

(1) Boerio, F. J.; Bahl, S. K.; McGraw, G. E. Vibrational Analysis of Polyethylene Terephthalate and Its Deuterated Derivatives. *J. Polym. Sci. Polym. Phys. Ed.* **1976**, *14* (6), 1029–1046. https://doi.org/10.1002/POL.1976.180140607.

(2) Sobhani, Z.; Al Amin, M.; Naidu, R.; Megharaj, M.; Fang, C. Identification and Visualisation of Microplastics by Raman Mapping. *Anal. Chim. Acta* **2019**, *1077*, 191–199. https://doi.org/10.1016/J.ACA.2019.05.021.

(3) Hernandez, E.; Nowack, B.; Mitrano, D. M. Polyester Textiles as a Source of Microplastics from Households: A Mechanistic Study to Understand Microfiber Release during Washing. *Environ. Sci. Technol.* **2017**, *51* (12), 7036–7046. https://doi.org/10.1021/ACS.EST.7B01750/SUPPL_FILE/ES7B01750_SI_001.PDF.

(4) Bond, T.; Ferrandiz-Mas, V.; Felipe-Sotelo, M.; van Sebille, E. The Occurrence and Degradation of Aquatic Plastic Litter Based on Polymer Physicochemical Properties: A Review. *Crit. Rev. Environ. Sci. Technol.* **2018**. https://doi.org/10.1080/10643389.2018.1483155.

(5) Rivera-Utrilla, J.; Bautista-Toledo, I.; Ferro-Garca, M. A.; Moreno-Castilla, C. Activated Carbon Surface Modifications by Adsorption of Bacteria and Their Effect on Aqueous Lead Adsorption. *J. Chem. Technol. Biotechnol.* **2001**, *76* (12), 1209–1215. https://doi.org/10.1002/JCTB.506.

(6) Srivastava, P.; Hasan, S. H. Biomass of Mucor Heimalis for the Biosorption of Cadmium from Aqueous Solutions: Equlibrium and Kinetic Studies. *BioRes.* **2011**, *6* (4), 3656-3675.